

Current-induced sliding motion in a helimagnet MnAu₂

Yuta Kimoto,^{1,*} Hidetoshi Masuda,¹ Takeshi Seki,^{1,2} Yoichi Nii,¹ and Yoshinori Onose¹

¹*Institute for Materials Research, Tohoku University, Sendai 980-8577, Japan*

²*Center for Science and Innovation in Spintronics (CSIS),
Core Research Cluster, Tohoku University, Sendai 980-8577, Japan*

We have found a signature of current-induced sliding motion in a helimagnet MnAu₂ thin film. In the helimagnetic state with a uniform chirality, differential resistivity shows an abrupt change at a threshold bias current. Judging from the similarity to the canonical charge/spin density wave systems, we have ascribed the abrupt change to the sliding motion of the helimagnetic structure. When the two chiral domains are equally mixed, the anomaly in the differential resistivity disappears, indicating the strong pinning effect of chiral domain wall.

In charge- or spin-ordered states, a large electric field sometimes drives the sliding motion of the ordered periodic structure. For example, in quasi-one-dimensional systems, charge/spin density wave (CDW/SDW) shows sliding motion under a large electric field [1, 2]. Theoretically, the sliding motion is described as the zero energy excitation in the gapless Goldstone (phason) mode [3] but, in reality, it is pinned by impurities and/or the commensurability, and therefore a certain magnitude of electric field is needed to drive the sliding motion. The differential resistivity, which is alternating current resistivity under a DC electric field, is abruptly decreased at the threshold DC electric field. The decrease is ascribed to the onset of sliding motion [1, 2]. Similar sliding phenomena have been observed in the Wigner crystal on liquid ⁴He surface [4] and strongly-correlated charge- and spin-ordered states in transition metal oxides [5].

In non-collinear magnetic structures, an electric current effectively drives the sliding motion because the transverse component of spin moment carried from the adjacent magnetic site induces a magnetic torque, which is denoted as spin-transfer torque (STT). For example, ferromagnetic domain wall is driven by an electric current larger than 10¹¹ A/m² in metallic case [6, 7] or 10⁸ A/m² in semiconducting case [8]. The topological non-collinear spin texture denoted as Skyrmion lattice also shows sliding motion by STT with much less threshold electric current [9–11].

Helical spin structure is one of the non-collinear magnetic structures. Many theoretical papers have predicted the sliding motion of helical spin structure [12–18]. The schematic image of the sliding motion of a helimagnetic structure is depicted in Fig. 1(a). When the electric current j is applied along the helical axis in a helical spin structure, the adiabatic STT expressed as $\tau_{\text{STT}} \propto (\mathbf{j} \cdot \nabla)\mathbf{S}$, in which \mathbf{S} is spatially dependent spin moment, tends to rotate the helical spin structure around the helical axis [19]. The collective rotation of helimagnetic structure corresponds to the sliding motion. While the picture of sliding motion in the helimagnetic structure is clear, experimental observation has not been reported yet. In this Letter, we report an experimental signature

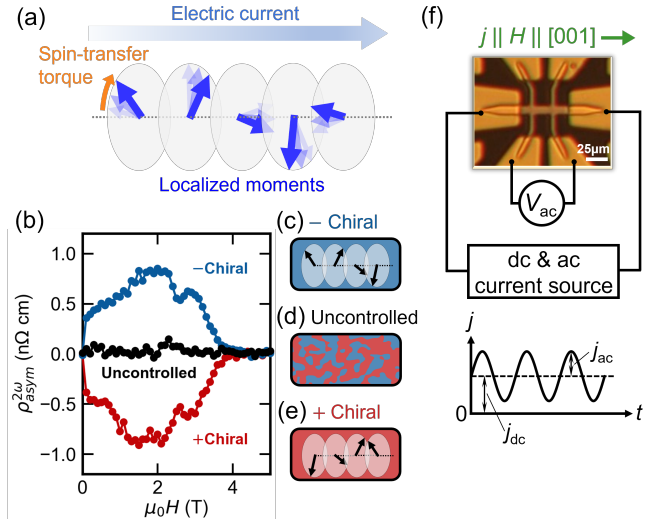


FIG. 1. (a) Schematic image of sliding motion of helimagnetic structure. (b) Nonreciprocal resistivity $\rho_{\text{asym}}^{2\omega}$ for \pm chiral and chirality-uncontrolled states at 250 K. (c)-(e) Schematic images of \pm chiral and chirality-uncontrolled states. (f) The experimental setup for the differential resistivity measurement.

of sliding motion in a helimagnet MnAu₂.

To observe the sliding motion of helical spin structure, we used single-crystalline helimagnetic MnAu₂ thin films. MnAu₂ (100 nm) were epitaxially grown on ScMgAlO₄ (10-10) substrates by sputtering. A capping layer of Ta (2 nm) was deposited on top of the MnAu₂ films as a protection layer. Hall bar devices with channel length 25 μm and width 10 μm [Fig. 1(f)] were fabricated using photolithography and Ar ion milling. The direction of electric current was parallel to the MnAu₂ [001] direction which is parallel to the helical propagation vector. The detail of the sample fabrication is shown in elsewhere [20]. Previously, Masuda *et al.* successfully controlled the chirality of helical spin structure in MnAu₂ thin films by the simultaneous application of an electric current and a magnetic field [20]. Similarly to their work, we confirmed that the chirality control also works for the present sample as shown in Fig. 1(b). We swept the magnetic field along the [001] direction from ± 5 T to 0 T with

an application of electric current ($j_0 = 8.0 \times 10^9$ A/m²) and then measured the nonreciprocal electronic transport that reflects the chirality. The sign of the nonreciprocal resistivity $\rho_{\text{asym}}^{2\omega}$, which is the field-asymmetric component of second harmonic resistivity, depends on whether the magnetic field and electric current applied prior to the measurement were parallel or antiparallel. This indicates the chirality was certainly controlled in the crystal. Here we define the chiral state controlled by the parallel electric current and magnetic field ($\mu_0 H = +5$ T) with negative $\rho_{\text{asym}}^{2\omega}$ as +chiral state and that controlled by the antiparallel magnetic field ($\mu_0 H = -5$ T) and current with positive $\rho_{\text{asym}}^{2\omega}$ as -chiral state. When the electric current was not applied, the nonreciprocal transport was negligible. This indicates that the magnetic domains with two chiralities coexisted as shown in Fig. 1(d). This state is denoted as chirality-uncontrolled state. Subsequent to the chiral domain control, we measured differential resistivity to observe the signature of the sliding motion. A DC and AC current source (Keithley 6221) was connected to the Hall-bar-shaped sample. The superposition of AC current ($j_{\text{ac}} = 0.505 \times 10^9$ A_{peak}/m², $f = 79.19$ Hz) and DC bias current j_{dc} were applied and the induced AC electric field E_{ac} was measured. Then, we obtained the differential resistivity $\rho_{xx} = \frac{E_{\text{ac}}}{j_{\text{ac}}}$ as a function of j_{dc} . In the following, we discuss the differential resistivity for three chiral domain states, +chiral state [Fig. 1(e)], -chiral state [Fig. 1(c)] and chirality-uncontrolled state [Fig. 1(d)].

Figure 2(a) exemplifies the real part of differential resistivities ρ_{xx} as a function of DC current density j_{dc} for the three chiral domain states in the helimagnetic state ($T = 250$ K, $\mu_0 H = 1.75$ T). Because the imaginary part of differential resistivity was always smaller than 0.2% of the real part in this work (see Supplemental Materials), hereafter we only show the real part of differential resistivity ignoring the imaginary part. In the chirality-uncontrolled state, ρ_{xx} shows quadratic j_{dc} dependence, which is attributed to the Joule heating. When the chirality is controlled, however, ρ_{xx} shows kinks around $j_{\text{dc}} = \pm 1.0 \times 10^9$ A/m² while it is almost independent of the sign of the chirality. To discuss the anomaly in the chirality-controlled states, we show in Fig. 2(b) the differences between ρ_{xx} in the chirality-controlled (\pm chiral) states and that in the chirality-uncontrolled state,

$$\Delta\rho_{xx} = \rho_{xx}(\pm\text{chiral}) - \rho_{xx}(\text{uncontrolled}). \quad (1)$$

The negative $\Delta\rho_{xx}$ in the low bias current region seems to be caused by the resistance of helimagnetic domain walls in the chirality-uncontrolled state. More importantly, $\Delta\rho_{xx}$ shows abrupt decreases at the threshold electric currents of $j_{\text{th}} \approx \pm 1.0 \times 10^9$ A/m². The chirality dependence of $\Delta\rho_{xx}$ was small and within the experimental uncertainty. It should be noted that similar abrupt decreases of differential resistivity have been reported in the CDW/SDW systems, which is ascribed to the sliding

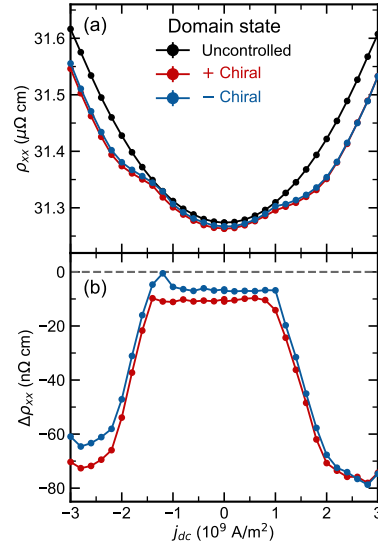


FIG. 2. (a) The differential resistivity in chirality-uncontrolled state (black) and chirality-controlled states with positive (red) and negative (blue) signs at 250 K and 1.75 T. (b) The differences between the differential resistivity in the chirality-controlled states and that in the uncontrolled state ($\Delta\rho_{xx}$) at 250 K and 1.75 T.

motion [1, 2].

To further delve into the anomaly of $\Delta\rho_{xx}$, let us discuss the magnetic field dependence. Figure 3(a) shows the bias current dependence of $\Delta\rho_{xx}$ for the +chiral state at various magnetic fields at 250 K. At 3.0 T, where the magnetic moments are forced to align ferromagnetically, $\Delta\rho_{xx}$ does not show discernible bias current dependence. On the other hand, all the $\Delta\rho_{xx}$ data show anomalies at some threshold bias current j_{th} in the helimagnetic state similar to the 1.75 T case (Figs. 2). The threshold bias current is almost minimum and $\Delta\rho_{xx}$ largely decreases at both the positive and negative threshold bias current at 1.75 T. As the magnetic field is increased from 1.75 T, the magnitude of the decrease in $\Delta\rho_{xx}$ gradually reduces, and at the same time, the threshold bias current increases. As the magnetic field is decreased from 1.75 T, the threshold bias current also increases and the change magnitude of $\Delta\rho_{xx}$ decreases.

In the lower magnetic field region, the bias current dependence in the positive bias current region becomes different from that in the negative bias current region. For example, at 1.25 T, $\Delta\rho_{xx}$ decreases at the positive threshold current but increases at the negative threshold current. Similar asymmetric bias dependence is observed in the low magnetic field region. In the whole magnetic field region, the data for the negative magnetic fields almost overlap with those for the positive magnetic fields, which indicates the present phenomena does

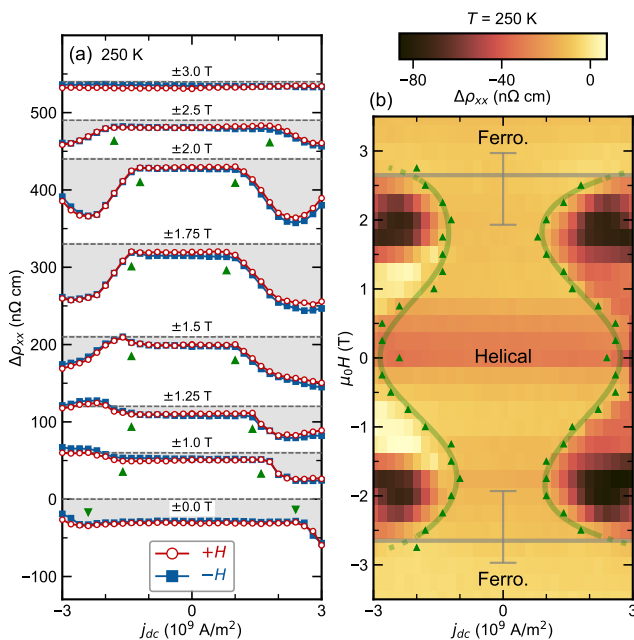


FIG. 3. (a) $\Delta\rho_{xx}$ for the +chiral state at various positive (red circles) and negative (blue squares) magnetic fields at 250 K. The green triangles denote threshold currents j_{th} at each magnetic field. (b) Contour mapping of $\Delta\rho_{xx}$ as a function of j_{dc} and magnetic field. The gray horizontal bars denote the helical-to-ferromagnetic phase transition field. The transitions are broad in the thin film sample presumably due to the epitaxial strain and the width of the transition field is shown as an error bar (for the details, see supplemental materials). The green triangles stand for j_{th} . The green lines are guides to the eyes.

not depend on the sign of a magnetic field. In addition, the dependence on the sign of chirality is quite small in the whole magnetic field range (see supplemental materials). Figure 3(b) shows the magnetic field dependence of the threshold bias current superimposed on the contour map of $\Delta\rho_{xx}$. When the magnetic field is increased from $\mu_0 H = 0$ T, the threshold bias current first decreases and then shows an upturn around 1.75 T. The magnetic field and bias current dependence of threshold bias current are almost symmetric.

Figure 4 shows the magnetic field dependence of threshold bias current with the contour map of $\Delta\rho_{xx}$ at various temperatures. At 350 K in the paramagnetic phase, $\Delta\rho_{xx}$ is almost absent. When the temperature is decreased from helimagnetic transition temperature $T_c \approx 343$ K, $\Delta\rho_{xx}$ begins to show an abrupt change at threshold currents. Overall, the threshold bias current increases with decreasing temperature. Below 175 K, the threshold current is larger than the maximum bias current in this experiment ($\pm 3.0 \times 10^9$ A/m²). The abrupt change of $\Delta\rho_{xx}$ is observed only in the helimagnetic state. Therefore, this phenomenon is obviously related to the helimagnetism. The temperature and magnetic field de-

pendence seem to reflect the variation of the magnetic state.

Let us discuss the origin of the abrupt change of ρ_{xx} . As mentioned above, the bias current dependence of $\Delta\rho_{xx}$ is quite similar to the bias voltage dependence of resistivity in CDW/SDW systems [1, 2]. In addition, this phenomenon is observed only in the helimagnetic state. These indicate that the abrupt change of ρ_{xx} is caused by the sliding motion of helimagnetic structure. While the sliding motion is caused by a voltage in CDW/SDW systems, STT induced by the application of electric current should drive the sliding motion in the present case. When the chirality is not controlled, the domain walls of two chiral states seem to strongly pin the magnetic structure and the sliding motion cannot be driven. On the other hand, when the chirality is controlled, the pinning force becomes weak and a large electric current steadily drives the sliding motion. The helimagnetic structure can be viewed as an infinite extension of the Bloch-type magnetic domain wall in a ferromagnet. The threshold electric current densities for the drive of magnetic domain walls were reported to be comparable with the present case [6, 8]. In the case of ferromagnetic domain walls, the magnetic anisotropy works as “intrinsic pinning” and tends to increase the threshold current density [7, 21, 22]. Similarly, the magnetic anisotropy seems to work against the sliding motion in the case of helimagnets [14]. The magnetic field perpendicular to the helical plane seems to weaken the magnetic field anisotropy and decrease the critical density while the canting of magnetic moments along the helical axis also decreases the effect of STT. The competition of these two effects may explain the magnetic field dependence of threshold bias current. The temperature dependence of threshold current may also be explained by the temperature variation of magnetic anisotropy.

Finally, let us discuss the asymmetric shape of $\Delta\rho_{xx}$ as a function of the bias current. $\Delta\rho_{xx}$ is almost independent of signs of chirality and magnetic field. Considering the centrosymmetric crystal structure of MnAu₂, the positive and negative current directions should be equivalent. At present, we cannot explain the asymmetry of bias current dependence of $\Delta\rho_{xx}$ appearing in the low magnetic field region. Perhaps, some inevitable tiny asymmetry of the experimental condition (device, field distribution, or something else) might cause the asymmetric current dependence, which seems to be exaggerated by the collective nature of sliding phenomenon while the tendency of bias current dependence was reproduced across samples.

In conclusion, we observed an abrupt change of differential resistivity at a threshold bias current in the helimagnetic state with a uniform chirality, which is ascribed to the sliding motion of helimagnetic structure. This indicates that the low-energy collective excitation is similar to the CDW/SDW system but the sliding motion of he-

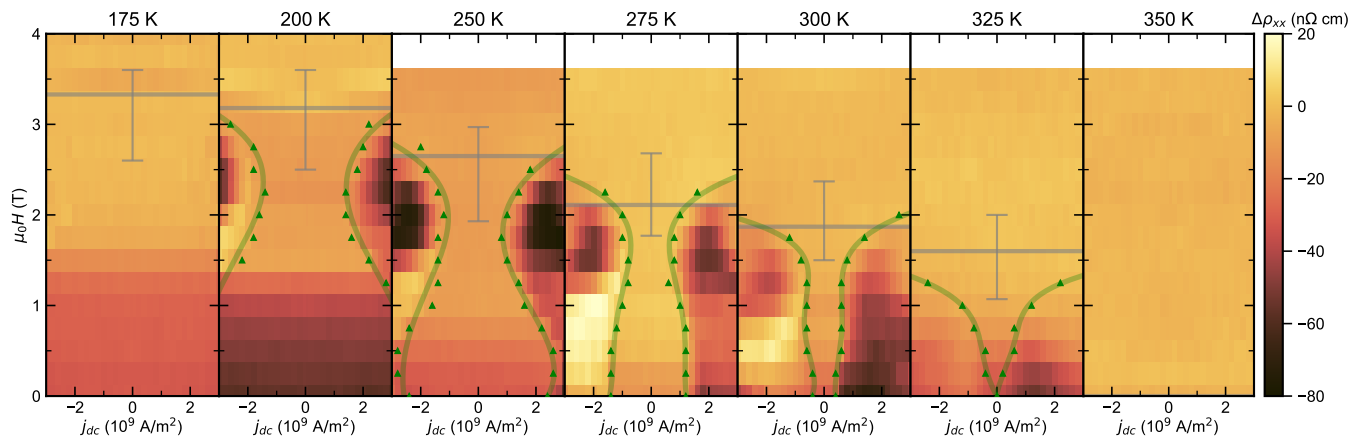


FIG. 4. Contour plot of $\Delta\rho_{xx}$ as functions of j_{dc} and magnetic field at various temperatures. The gray horizontal bars denote the helical-to-ferromagnetic phase transition fields. The transitions are broad in this thin film sample presumably due to the epitaxial strain and the width of transition field is shown as an error bar (for the details, see supplemental materials). The green triangle symbols stand for j_{th} . The green lines are guides to the eyes.

limagnetic structure is driven by an electric current not by an electric field. The magnetic structure manipulable with an electric current seems to be useful for the race track memory [23, 24]. In this sense, this work might pave an avenue for the helimagnet-based spintronics.

We appreciate T. Sasaki for her help in the film deposition. The film deposition and device fabrication were carried out at the Cooperative Research and Development Center for Advanced Materials, IMR, Tohoku University. This work was supported by JSPS KAKENHI(Grants No. JP20K03828, No. JP21H01036, No. JP22H04461, No. JP23H00232 and No. JP23K13654), JST SPRING(Grant No. JPMJSP2114), JST PRESTO (Grant No. JPMJPR19L6), and the Mitsubishi Foundation. Y.K. acknowledges support from GP-Spin at Tohoku University.

* yuta.kimoto.t7@dc.tohoku.ac.jp

- [1] G. Grüner and A. Zettl, *Physics Reports* **119**, 117 (1985).
- [2] G. Grüner, *Rev. Mod. Phys.* **66**, 1 (1994).
- [3] P. A. Lee, T. Rice, and P. W. Anderson, *Solid State Communications* **14**, 703 (1974).
- [4] K. Shirahama and K. Kono, *Phys. Rev. Lett.* **74**, 781 (1995).
- [5] S. Yamanouchi, Y. Taguchi, and Y. Tokura, *Phys. Rev. Lett.* **83**, 5555 (1999).
- [6] A. Yamaguchi, T. Ono, S. Nasu, K. Miyake, K. Mibu, and T. Shinjo, *Phys. Rev. Lett.* **92**, 077205 (2004).
- [7] T. Koyama, D. Chiba, K. Ueda, K. Kondou, H. Tanigawa, S. Fukami, T. Suzuki, N. Ohshima, N. Ishiwata, Y. Nakatani, K. Kobayashi, and T. Ono, *Nature Mater* **10**, 194 (2011).
- [8] M. Yamanouchi, D. Chiba, F. Matsukura, and H. Ohno, *Nature* **428**, 539 (2004).
- [9] F. Jonietz, S. Mühlbauer, C. Pfleiderer, A. Neubauer, W. Münzer, A. Bauer, T. Adams, R. Georgii, P. Böni, R. A. Duine, K. Everschor, M. Garst, and A. Rosch, *Science* **330**, 1648 (2010).
- [10] T. Schulz, R. Ritz, A. Bauer, M. Halder, M. Wagner, C. Franz, C. Pfleiderer, K. Everschor, M. Garst, and A. Rosch, *Nature Phys* **8**, 301 (2012).
- [11] T. Yokouchi, S. Hoshino, N. Kanazawa, A. Kikkawa, D. Morikawa, K. Shibata, T.-h. Arima, Y. Taguchi, F. Kagawa, N. Nagaosa, and Y. Tokura, *Science Advances* **4**, eaat1115 (2018).
- [12] Y. Tserkovnyak and A. Brataas, *Phys. Rev. B* **71**, 052406 (2005).
- [13] O. Wessely, B. Skubic, and L. Nordstrom, *Phys. Rev. Lett.* **96**, 256601 (2006).
- [14] O. Wessely, B. Skubic, and L. Nordstrom, *Phys. Rev. B* **79**, 104433 (2009).
- [15] J. Iwasaki, M. Mochizuki, and N. Nagaosa, *Nat Commun* **4**, 1463 (2013).
- [16] N. Del Ser, L. Heinen, and A. Rosch, *SciPost Phys.* **11**, 009 (2021).
- [17] V. V. Ustinov and I. A. Yasyulevich, *Phys. Rev. B* **106**, 064417 (2022).
- [18] D. Kurebayashi, Y. Liu, J. Masell, and N. Nagaosa, *Phys. Rev. B* **106**, 205110 (2022).
- [19] A. Brataas, A. D. Kent, and H. Ohno, *Nature Mater* **11**, 372 (2012).
- [20] H. Masuda, T. Seki, Y. Nii, H. Masuda, K. Takanashi, and Y. Onose, (2022), [arXiv:2205.13112 \[cond-mat.mes-hall\]](https://arxiv.org/abs/2205.13112).
- [21] L. Berger, *Journal of Applied Physics* **71**, 2721 (1992).
- [22] G. Tatara and H. Kohno, *Phys. Rev. Lett.* **92**, 086601 (2004).
- [23] S. S. P. Parkin, M. Hayashi, and L. Thomas, *Science* **320**, 190 (2008).
- [24] R. Tomasello, E. Martinez, R. Zivieri, L. Torres, M. Carpentieri, and G. Finocchio, *Sci Rep* **4**, 6784 (2014).

Supplemental material for:
Current-induced sliding motion in a helimagnet MnAu_2

Yuta Kimoto,^{1,*} Hidetoshi Masuda,¹ Takeshi Seki,^{1,2} Yoichi Nii,¹ and Yoshinori Onose¹

¹*Institute for Materials Research, Tohoku University, Sendai 980-8577, Japan*

²*Center for Science and Innovation in Spintronics (CSIS),
Core Research Cluster, Tohoku University, Sendai 980-8577, Japan*

arXiv:2403.00167v1 [cond-mat.mtrl-sci] 29 Feb 2024

* yuta.kimoto.t7@dc.tohoku.ac.jp

ANALYSIS OF HALICAL-TO-FERROMAGNETIC TRANSITION FIELD.

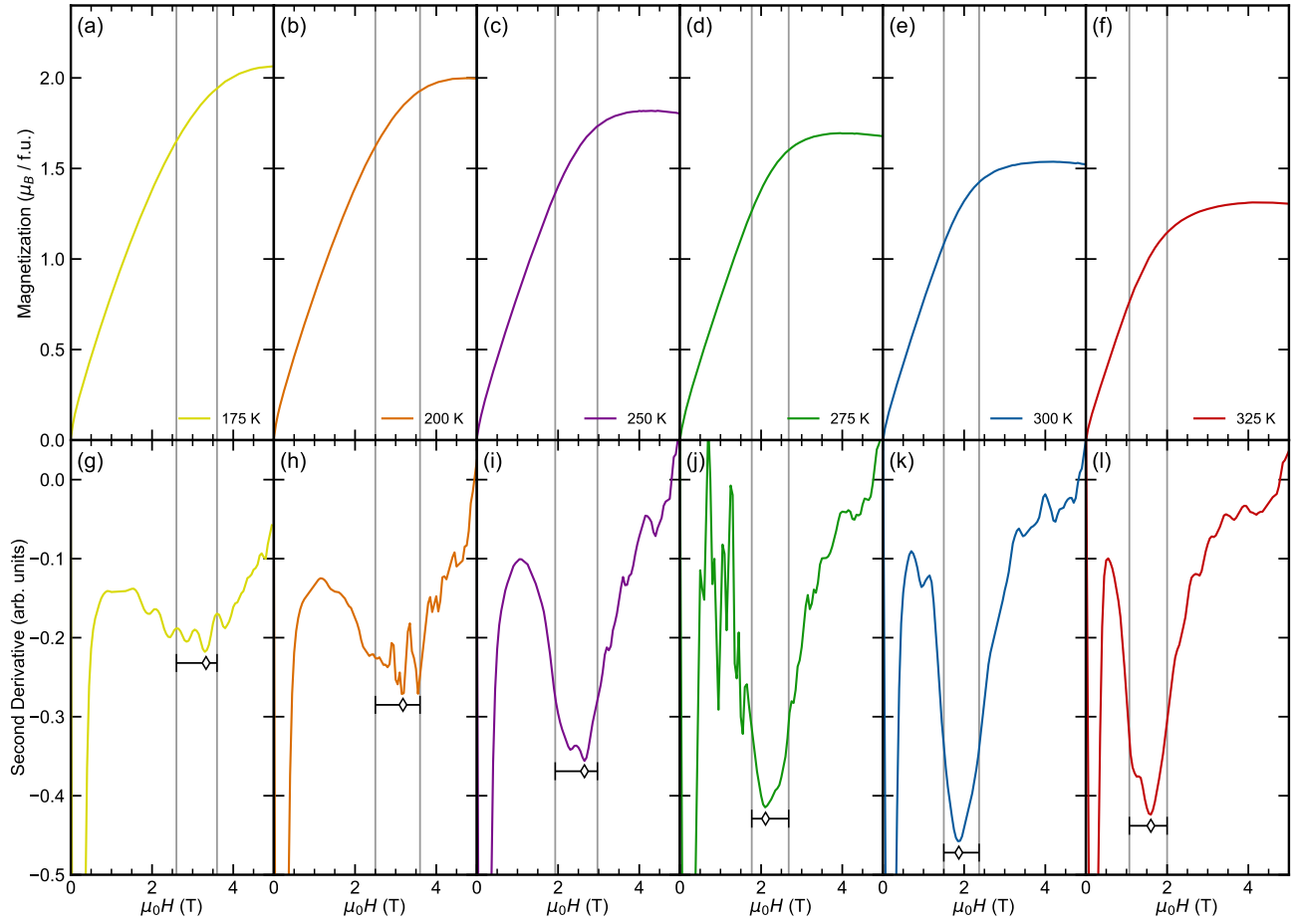


FIG. S1. (a)-(f) Magnetization curves at various temperatures in the MnAu_2 thin film. The diamagnetic component of ScMgAlO_4 substrate is subtracted. (g)-(l) The second derivative of the magnetization curves shown in the FIG. S1(a)-(f). The negative broad peak is caused by the helimagnetic-to-ferromagnetic transition. In the thin film, the transition is a little bit broad perhaps due to the epitaxial strain. The transition field is estimated as the peak and the width is estimated as the width of two-thirds maximum, which is plotted as the error bars in these figures as well as in Fig. 3(b) and Fig. 4 in the main text.

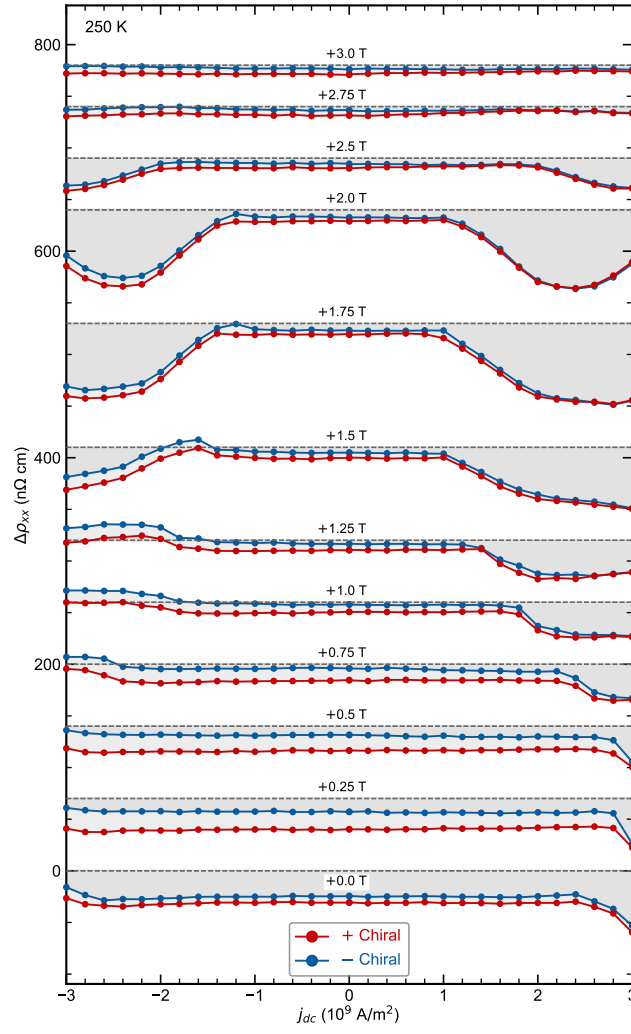
COMPARISON OF $\Delta\rho_{xx}$ FOR TWO CHIRAL STATES.

FIG. S2. $\Delta\rho_{xx}$ as a function of j_{dc} for both two chiral states at various magnetic fields. The small difference between two chiral states is mainly caused by the slight difference of measurement temperature.

COMPARISON OF REAL AND IMAGINARY PARTS OF ρ_{xx}
AT VARIOUS MAGNETIC FIELDS AT 250 K.

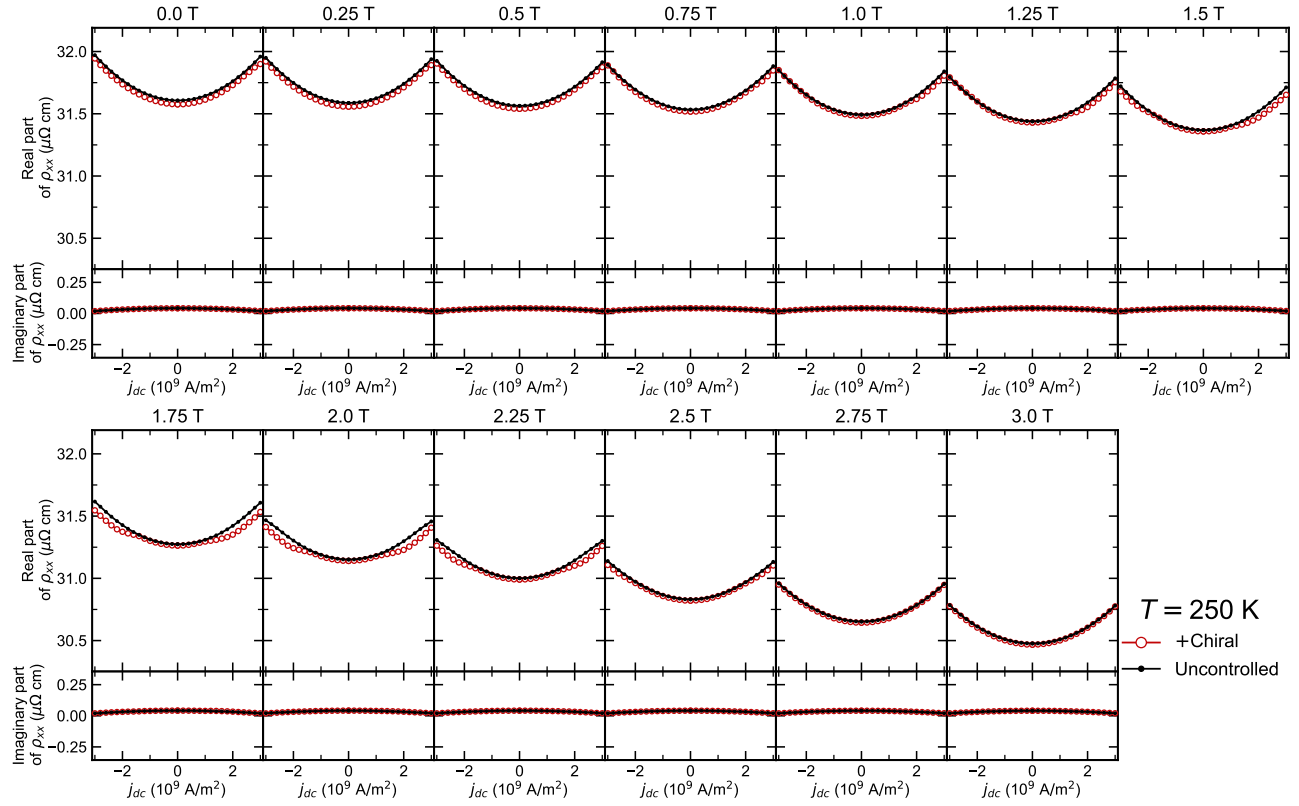


FIG. S3. The real and imaginary parts of ρ_{xx} as a function of j_{dc} at 250 K. The magnitude of imaginary part is smaller than 0.2% of the real part for all the magnetic field data.

FULL LINE PLOTS OF $\Delta\rho_{xx}$ AT VARIOUS TEMPERATURES.

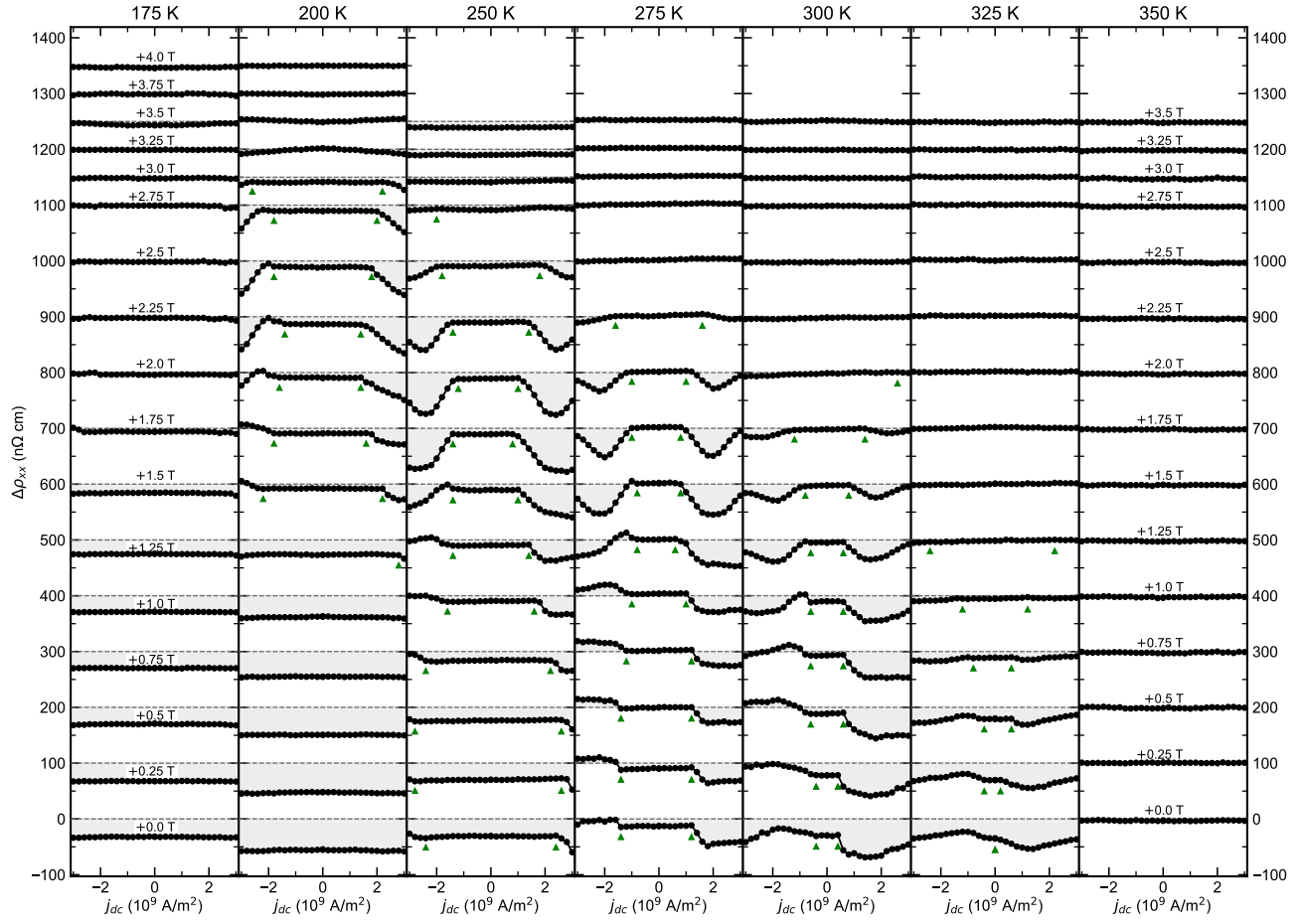


FIG. S4. $\Delta\rho_{xx}$ as a function of j_{dc} at various magnetic fields and temperatures, which are shown as contour plots in Figure 4 in the main text. The green triangles denote the threshold currents j_{th} .